Energy Research and Development Division
FINAL PROJECT REPORT

PRELIMINARY ASSESSMENT OF OFFSHORE WIND DEVELOPMENT IMPACTS ON MARINE ATMOSPHERIC ENVIRONMENT

Prepared for: California Energy Commission
Prepared by: Department of Atmospheric and Oceanic Sciences, UCLA

MARCH 2015
CEC-500-2016-023

PREPARED BY:

Primary Authors:
Hsin-Yuan Huang
Alex Hall

UCLA Department of Atmospheric and Oceanic Sciences
Box 951565
405 Hilgard Ave.
Los Angeles, CA 90095
Phone: 310-206-5253
http://web.atmos.ucla.edu/csrl/

Contract Number: 500-11-033

Prepared for:

California Energy Commission

Lillian Mirviss
Joe O'Hagan
Contract Manager

Aleecia Gutierrez
Office Manager
Energy Generation Research Office

Laurie ten Hope
Deputy Director
Energy Research & Development Division

Robert Oglesby
Executive Director

ACKNOWLEDGEMENTS

The authors would like to thank Patrick Volker, Wind Energy Department at Technical University of Denmark, Scott Capps, Vertum Partners, and Lionel Renault, UCLA Department of Atmospheric and Oceanic Sciences, for their contributions to this project. The authors would also like to thank the California Energy Commission and California Institute of Energy and Environment for the project's financial support.

PREFACE

The California Energy Commission Energy Research and Development Division supports public interest energy research and development that will help improve the quality of life in California by bringing environmentally safe, affordable, and reliable energy services and products to the marketplace.

The Energy Research and Development Division conducts public interest research, development, and demonstration (RD&D) projects to benefit California.

The Energy Research and Development Division strives to conduct the most promising public interest energy research by partnering with RD&D entities, including individuals, businesses, utilities, and public or private research institutions.

Energy Research and Development Division funding efforts are focused on the following RD&D program areas:

- Buildings End-Use Energy Efficiency
- Energy Innovations Small Grants
- Energy-Related Environmental Research
- Energy Systems Integration
- Environmentally Preferred Advanced Generation
- Industrial/Agricultural/Water End-Use Energy Efficiency
- Renewable Energy Technologies
- Transportation

Preliminary Assessment of Offshore Wind Development Impacts on Marine Atmospheric Environment is a final report for the *Exploratory Studies of Potential Environmental Issues with Alternative Energy Futures for California* project (contract number 500-11-033) conducted by the University of California, Los Angeles Department of Atmospheric and Oceanic Sciences. The information from this project contributes to Energy Research and Development Division's Energy-Related Environmental Research Program.

When the source of a table, figure or photo is not otherwise credited, it is the work of the author of the report.

For more information about the Energy Research and Development Division, please visit the Energy Commission's website at www.energy.ca.gov/research/ or contact the Energy Commission at 916-327-1551.

ABSTRACT

California seeks to increase renewable energy production in the near future, and utilizing large-scale offshore wind farms provides an alternative to sacrificing scarce land to meet this end. However, the impacts of offshore wind farms on the marine atmospheric environment should be understood before any decisions about wind farm placement are made. Using a high-resolution regional climate model supplemented by a wind farm parameterization, the authors investigated the atmospheric effects of a hypothetical offshore wind farm located in a region with sufficient wind resources near Northern California's major metropolitan areas. The hypothetical wind farm, which uses large-scale, modern turbines, would provide electricity for more than 750,000 households in the Bay Area. The reference simulation, which reproduces the local micrometeorology accurately in comparison with observations, predicts that the hypothetical offshore wind farm would affect the near-surface atmospheric environment differently than an onshore wind farm would. Specifically, an offshore wind farm would introduce a vertical mixing mechanism that has a cooling effect on the marine boundary layer, causing a decrease in air temperature and an increase in air humidity. The additional moisture caused by the wind farm would subsequently condense into liquid water and form clouds at the top of the boundary layer. As they combine with the influence of wind farm–induced wake, these clouds would affect incoming radiative fluxes, surface energy budget, and the resulting surface turbulent fluxes in various ways.

Keywords: California offshore wind farm, wind energy, environmental impacts, atmospheric boundary layer

Please use the following citation for this report:

Huang, Hsin-Yuan, and Alex Hall (UCLA Department of Atmospheric and Oceanic Sciences). 2015. *Preliminary Assessment of Offshore Wind Development Impacts on Marine Ecosystems.* California Energy Commission. CEC-500-2016-023.

TABLE OF CONTENTS

LIST OF FIGURES

LIST OF TABLES

EXECUTIVE SUMMARY

Introduction

As California seeks to increase renewable energy production within the state, the significant offshore wind resources, which are much greater than those found onshore, are receiving increased attention. However, the effects of offshore wind farms on the marine atmospheric environment must be understood before any decisions about wind farm placement are made.

Wind turbines generate electrical power by extracting energy from the motion of air flow through the turbine. As wind blows past a wind turbine, wind speeds are reduced downwind. Recent studies have found that onshore wind farms containing small turbines significantly increase atmospheric mixing and near-surface warming. In comparison, larger offshore turbines create even more mixing. This same mixing mechanism creates different meteorological impacts over the sea surface than it does over land. California's coast is a region of ocean upwelling driven by consistent northerly winds. Changes in atmospheric structure downwind from a large offshore wind farm could potentially alter ocean thermal structure, upwelling, nutrient supply, and probably the marine ecosystem.

Project Purpose

Using a high-resolution regional climate model supplemented with numerical parameters representing a wind farm, the researchers investigated the atmospheric effects of a hypothetical offshore wind farm located in a region with sufficient wind resources near Northern California's major metropolitan areas.

Wind Farm

The researchers developed an advanced wind farm simulation model that describes the flow distortion from wave farm operation and is operated in the latest version of the Weather Research and Forecasting (WRF) model, a regional atmospheric model. Since the model grid spacing in this atmospheric model is on the order of 2 km, the energy extracted by turbines and the wake development inside the grid cells that contain the turbines are numerically characterized just as other atmospheric processes are rather than described explicitly.

Weather Research and Forecasting Simulations

The regions selected for the study are void of any exclusion zones, have sufficient wind resources, and are located near the San Francisco Bay Area, a major metropolitan region. The size of the simulated wind farm is comparable to current offshore wind farms that are slated for development within the North Sea in Europe. To detect the atmospheric impacts of the wind farm, the researchers ran two WRF simulations spanning the year of 2009: a "reference" WRF simulation with no wind farm and an "experiment" simulation with the wind farm.

The WRF resolution and configuration selected for this study represent the local meteorology accurately. The WRF reference simulation is first evaluated against point-scale observations (such as the buoy measurements provided by the National Oceanic and Atmospheric Administration's National Data Buoy Center) in terms of reference-level wind speed, air temperature, and stability. Then the distribution of near-surface wind speed against remotely

sensed data from QuikSCAT, an Earth observation satellite that records sea-surface wind speed and direction data, was compared. Overall, good agreement is seen between the WRF outputs and both the point-scale observations and the remotely-sensed products. Thus, the researchers feel confident in using the realistic, high-resolution WRF data to further investigate the impacts of a large-scale wind farm on the marine boundary layer system.

Project Results

Due to an increase in vertical mixing, the hypothetical wind farm induces a cooling effect on the atmospheric environment, increasing the amount of water vapor in the air and decreasing air temperature in the lower marine boundary layer, which is the part of the atmosphere directly affected by the ocean. Meanwhile, the wind turbines extract energy as wind flows through the wind farm, causing a significant reduction in wind speed (as well as shear stress). The reduction in wind speed is up to 10 percent at the center of wind farm, and the range of reduced winds more than 100 km downstream.

When the wind turbines increase the vertical mixing in marine boundary layer, the top of the boundary layer rises, transporting more water vapor from the sea surface. As a result, more air moisture accumulates at a higher boundary layer top and forms more clouds. These results show that the increased clouds mainly concentrated above the location of wind farm and nearby downstream. Since solar radiation is reflected by clouds, the major effect of these additional clouds is to reduce the incoming solar energy reaching the ocean surface, further affecting the ocean surface energy budget. The wind farm–induced wakes due to wind speed reduction can extend more than 100 km downstream. The distributions of changes in air temperature and humidity basically follow the wake propagation and further affect the distributions of surface turbulent fluxes. This finding matches a recent laboratory experiment study by Zhang et al. (2013).

In this project, the researchers investigated the potential effects of a large-scale modern offshore wind farm located near Northern California's coast on the surrounding atmospheric environment. The WRF model, integrated with a recently developed numerical simulation of a wind farm, was used to perform simulations. Because cooler, more humid air is mixed upwards in the atmospheric boundary layer, a decrease in air temperature occurs. This result matches the global observations of wind farms reported in Wang and Prinn (2011).

Furthermore, because of a strong inversion with frequent stratocumulus clouds over the study area, the additional water vapor brought by the wind turbines lead to more water condensation and cloud formation.

Project Benefits

The results of this research benefit California ratepayers by identifying potential atmospheric effects from large scale-wind energy development off the state's coastline. Since offshore wind presents such an abundant renewable energy resource, understanding the consequences of developing such energy resources is important to future siting of this renewable energy resource.

CHAPTER 1:
Introduction

Development of clean and renewable energy sources is necessary to reduce dependence on fossil fuels while mitigating climate change and pollution. Wind energy is one of the cleanest resources among various renewable energy technologies available today (Jacobson 2009). Most wind farms in the United States are currently installed on shore, and the development of offshore wind farms has been neglected due to the high costs and difficulties associated with installation and maintenance. However, there are extensive developments of offshore wind farms throughout Northern Europe (such as in the North Sea). Because land with viable wind resources is limited in California, developing offshore wind farms is inevitable if more wind energy is to be (USDoE, 2008; Jacobson et al., 2014).

Thanks to recent engineering advances, wind turbine performance has significantly improved, reducing costs over the past decade. Larger and more powerful turbines will be available within the next 30 years; however, due to their size, these turbines cannot be erected on shore. This is because the standard widths of the state's roads and bridges place constraints on the size of the turbine components that manufacturers can deliver over them.

That said, there are some foreseeable factors will help California gradually overcome the large economic barrier associated with harnessing its offshore wind resources. The increased productive capacity of future turbines will likely outweigh the added costs of building more offshore wind farms (Weinzettel et al., 2009). Furthermore, winds over the ocean are typically stronger and less turbulent than those over the land, equating to less wear-and-tear on the turbine and lengthening the turbine life (Barthelmie and Pryor, 2006). Finally, the possibility of building more onshore wind farms is lessening as the amount of land with viable wind resources decreases and exclusion zones spread.

Making fully informed decisions regarding the placement of offshore wind farms along any coast requires not only an understanding of wind magnitude distribution, but also an understanding of wind farm–induced impacts on environmental properties, especially for those inside the atmospheric boundary layer (Baidya Roy, 2010; Wang and Prinn, 2011; Fitch et al., 2012). Therefore, the objective of this study is to answer the question: *What is the key impact of a hypothetical large-scale wind farm located off a coast on its surrounding atmospheric environment?* California was chosen as a test case in part because it hosts a rich marine ecosystem driven by the same alongshore-flowing winds that make it a potentially valuable wind energy resource.

Recently, a few studies (such as Schwartz et al., 2010; Dvorak et al., 2010) have used atmospheric models to provide preliminary assessments of wind power resources in California. However, these frameworks may not be able to realistically simulate wind farm–induced impacts because they do not simulate the action of turbines in a large-scale wind farm. A subgrid-scale turbine-induced wake parameterization is also necessary to obtain an accurate wind power assessment, which requires wind statistics across the entire turbine rotor swept area (Wagner et al., 2008; Wharton and Lundquist, 2010; Fitch et al., 2012). Recently, two

modeling approaches have become widely used to represent wind turbines and to simulate their impacts on local or regional micrometeorology. The first is the use of large-eddy simulation models (Calif et al., 2010, 2011; Lu and Porté-Agel, 2011; Churchfield et al., 2012). The key advantage of large-eddy simulation is it provides statistical details in turbulent characteristics and meteorological variables. The second approach is the use of a mesoscale model integrated with a wind turbine module (Baidya Roy et al., 2004; Baidya Roy and Traiteur, 2010; Fiedler and Bukovsky, 2011; Fitch et al., 2012, 2013). This method can be applied to simulate a realistic regional atmospheric environment and to investigate wind farm–induced impacts for a large domain. In this study, the researchers perform numerical experiments using a framework that includes a modern regional climate model implemented with a recently developed wind farm parameterization. Simulations are expected to accurately assess wind power using turbine characteristics, including power curve and blade length, and to realistically represent the impacts of the offshore wind farm on the atmospheric boundary layer characteristics like temperature humidity, and cloud formation.

In the following sections, the authors first briefly describe the wind farm parameterization and experimental design and offer a preliminary evaluation of the hypothetical model performance. Then, the energy production of the hypothetical wind farm is identified and the wind farm's environmental impacts on meteorological properties are analyzed. In the last section, key findings are summarized.

CHAPTER 2:
Numerical Experiments

The model structure and numerical experiments are described in this chapter.

2.1 Windfarm parameterization

Simulations in this study are performed using the WRF model (Skamarock et al., 2008) version 3.4 with the implementation of a recently developed wind farm parameterization (Volker et al., 2014), originally introduced by the Department of Wind Energy at Technical University of Denmark. Designed as a subgrid-scale parameterization in a mesoscale model, this wind farm scheme describes the unresolved wind turbine–induced wake expansion explicitly based on the classic far wake theory (Wyngaard, 2010). Assuming the vertical profile of turbine-induced velocity deficit follows a Gaussian distribution, the grid-averaged maximum velocity deficit at wind turbine hub height is described as:

$$\overline{U}_S = \sqrt{\frac{\pi}{2}} \frac{C_T R_0^2 U_0}{2\Delta y \bar{\sigma}}, \quad (1)$$

where C_T is the thrust coefficient, R_0 is wind turbine rotor radius, U_0 is free upstream wind velocity, Δy is the wake width in the cross-stream direction, and $\bar{\sigma}$ is a spatial-averaged length scale determining the vertical wake extension. The shape of the vertical velocity deficit matches the results of laboratory wind tunnel experiments and large-eddy simulation studies (Chamorro and Porté-Agel, 2010; Porté-Agel et al. 2011; Wu and Porté-Agel, 2011). The reader is referred to Volker et al. (2014) for more details about this wind farm parameterization and its performance against observations collected at the Horns Rev I wind farm in the North Sea.

2.2 Simulation setup

An offshore region with sufficient wind resources exists to provide wind power energy for major metropolitan areas in Northern California like the San Francisco Bay Area is selected in this study. The WRF simulation domain was designed to cover a large region of the Northern California coast so that the northerly wind flows can be captured consistently (Schwartz et al., 2010) through the location of the hypothetical wind farm. The innermost simulation domain, with a 2-km resolution, is shown in Figure 1a, in which the black rectangle, blue circles, and cyan squares represent the locations of the wind farm, buoy stations, and major cities, respectively. The hypothetical wind farm consists of 200, eight-megawatt, 125 m hub height Vestas V164 wind turbines (Vestas, 2013), which were tested at Østerild station in Denmark in 2013 and became operational in 2014.

Figure 1: a) Part of the WRF Inner Domain With Terrain Contours (m) and b) Annual Mean of Hub-Height (125 m) Wind Field (m/s)

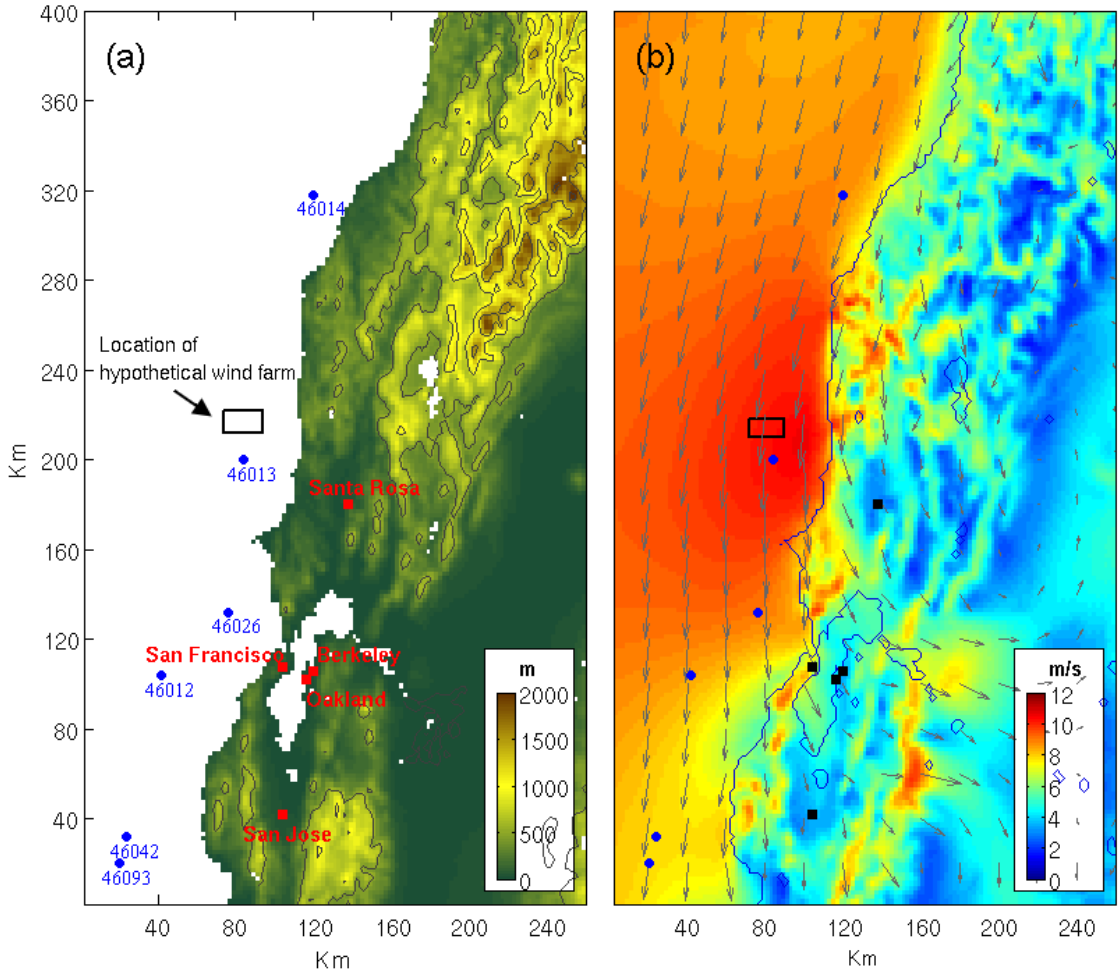

In panel a), locations of major cities and buoy stations are presented as blue circles and red squares, respectively. The black box is the location of hypothetical wind farm in both panels.

The three-hourly, 32-km resolution North American Regional Reanalysis data[1] (Mesinger et al., 2006) provided by the National Centers for Environmental Prediction are used as the initial and boundary conditions for the simulations. To detect the wind farm-induced impacts on the surrounding environment, two one-year-long simulations – a "reference" simulation without the wind farm and an "experiment" simulation with the wind farm – are initialized at 0000 UTC on January 1, 2009. Key physical schemes and parameterizations (e.g., radiation, microphysics, and boundary layer) selected for the simulations are listed in Table 1. These WRF physical schemes have been similarly configured in previous studies such as Huang et al., 2013 and Jousse et al., 2014. These studies show that WRF can reproduce the stratocumulus marine boundary layer over the study domain well.

[1] http://www.esrl.noaa.gov/psd/data/gridded/data.narr.html

Table 1: List of Key Physical Models and Parameterizations Used for WRF Simulations

Scheme	Name	Selected reference
Shortwave radiation	Dudhia	Dudhia (1989)
Longwave radiation	Rapid Radiative Transfer model (RRTM)	Mlawer *et al.* (1997)
Microphysics	WRF single-moment 6-class	Hong and Lim (2006)
Cumulus	Kain-Fritsch (Eta scheme)	Kain (2004)
Boundary-layer	Mellor-Yamada-Nakanishi-Niino (MYNN)	Nakanishi and Niino (2004)
Land surface	Noah land surface model	Chen and Dudhia (2001)

As shown in Figure 1b, hub-height (125 m above sea surface) wind meteorology is well reproduced in the reference simulation. The ocean region is dominated by persistent northerly winds. Due to topographic effects, offshore winds turn slightly inland when they reach the San Francisco Bay Area. Though wind speeds generally slow over land, significantly stronger winds are seen in narrow channels near major mountain passes. The strongest onshore winds are seen in the Altamont Pass, where one of the earliest onshore wind farms in the U.S. is located. The hypothetical wind farm (black box) is located within a region that has the strongest offshore winds inside the simulation domain. It is also located close to shore since this allows for electricity generated from the offshore wind farm to be transmitted to inland along a short route (Dvoraka et al., 2010).

2.3 Evaluation of near-surface wind and temperature

Monthly wind rose plots are illustrated in Figure 2, which shows the wind speed and wind direction blowing through the wind farm location in the reference simulation. These wind rose plots show that faster winds are seen during spring and summer, whereas slower winds are seen in autumn and winter. For the study domain, the strongest winds over the designed wind farm occur between March and May. During this period, daily mean wind speed is generally larger than 12 m/s. Winds consistently blow in a southeastward direction year-round, except during the winter months from December to February. This is because, along California's coast, winds blowing offshore during precipitation events (usually in winter) occasionally disturb the normal wind regime. Detailed analysis shows the dominant wind direction blowing through the wind farm is about 270° (counterclockwise from east). Therefore, only wind events with a direction in the range of 270°±10° were selected to clarify the impacts of the wind farm on the downstream environment. The fraction of selected ensembles is about 78 percent of the total wind events in the simulation.

Figure 2: Monthly Wind Rose Plots Over the Designed Wind Farm in the Reference Simulation

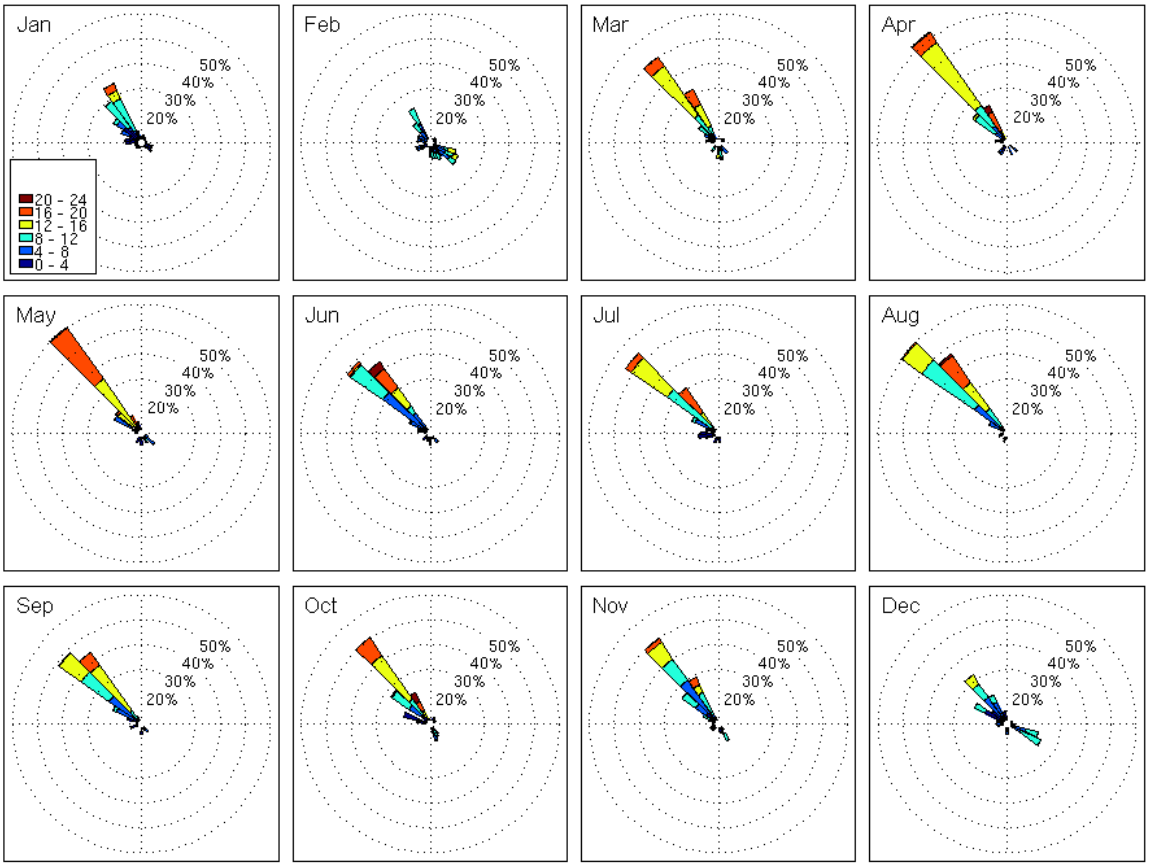

Plots use the meteorological convention for winds with unit of m/s.

To illustrate model performance, simulated near-surface wind speed and air temperature at the reference level are compared against observations collected at National Oceanic and Atmospheric Administration buoy stations[2] shown in Figure 3. To facilitate a fair comparison, simulated outputs are extrapolated from the lowest model level down to the respective buoy anemometer height based on the model's surface layer physics. Marker locations designate the mean values over the simulation period, and their colors represent the correlation coefficient between model outputs and observations. Comparison shows reasonable agreement between simulated wind speed and observational data (Figure 3a). For most stations, differences between WRF-simulated and observed wind speeds are less than 6 percent, with a correlation coefficient larger than 0.7. Similarly strong agreement is also seen in the air temperature comparison (Figure 3b).

[2] http://www.ndbc.noaa.gov/

Figure 3: Comparisons of Near-Surface a) Wind Speed (m/s) and b) Air Temperature (°C) Between WRF-Simulated Outputs at the Nearest Grid Points From the Reference Simulation and Observations Collected at National Oceanic and Atmospheric Administration Buoy Stations (Numbered in Text)

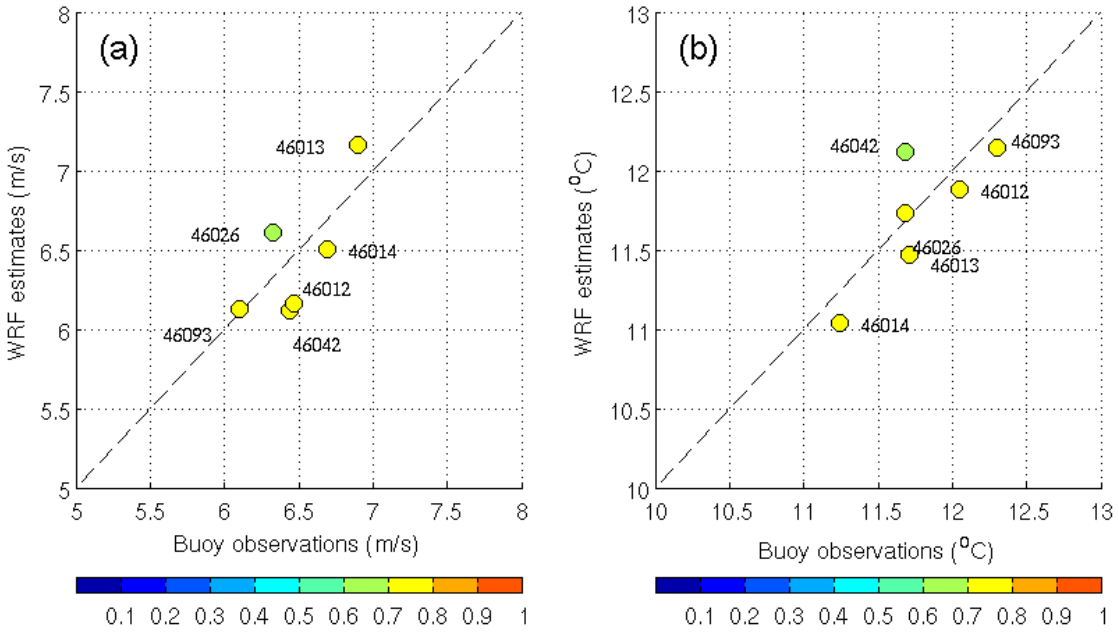

Marker locations designate the means over the simulation period, and their colors represent the correlation coefficient (scale shown in the colorbar below each graph).

Spatial pattern comparison of averaged wind speed from QuikSCAT[3] observed and WRF is presented in Figure 4. Only the nearest in time model outputs to the satellite overpasses are selected for a fair comparison. Due to grid resolution differences between the remotely-sensed data (12.5 km) and the dynamical simulation (2 km), a simple linear interpolation is used to upscale WRF outputs in order to compare against QuikSCAT products. WRF simulation results (Figure 4a), in general, compare well to QuikSCAT observations (Figure 4b) in both wind speed magnitude and spatial distribution. Slightly larger differences (between QuikSCAT data and WRF output) are seen on the upper and left boundaries of study domain (Figure 4c). This might be because of numerical error from interpolation method at boundary. Differences inside the simulation domain are relatively low (less than 1 m/s). Similar results are also seen in the root-mean-square error plot shown in Figure 4d.

Based on these promising results, the authors have confidence that these high-resolution WRF data can be used to make a reasonable assessment of the wind farm-induced impacts on the surrounding environment.

[3] http://manati.star.nesdis.noaa.gov/datasets/QuikSCATData.php

Figure 4: Comparison of Averaged Wind Speed Between WRF Outputs and QuikSCAT Observations: a) QuikSCAT, b) WRF Simulation, c) Difference, and d) Root-Mean-Square Error

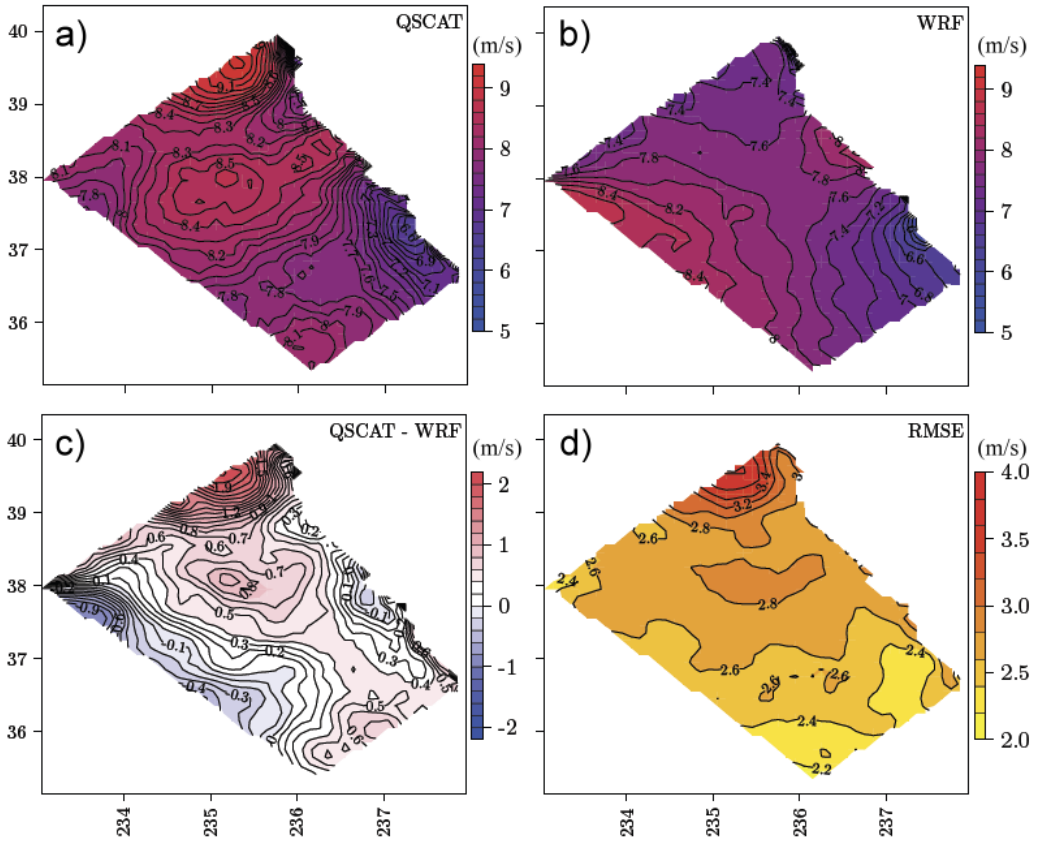

CHAPTER 3:
Impacts on Atmospheric Environment

3.1 Wind energy production

Ensemble averages of hub-height wind speed and turbulent kinetic energy (TKE) in the reference (without wind farm, blue line) and experiment (with wind farm, red line) simulations are shown in Figure 5. The green line represents the percentage of difference between the two simulations (i.e., experiment–reference) and the gray area is the location of wind farm. Because the wind farm acts as a porous media for wind flows to increase pressure (not shown), wind speed significantly decreases when the air flows blow through the wind farm (Figure 5a). Divergence in hub-height wind speed starts about 20 km ahead of the wind farm. This pressure increase (wind speed decrease) may affect the vertical transport of meteorological variables and in turn the marine boundary layer structure, which will be investigated later. Meanwhile, in addition to a sink of momentum, the subgrid wind farm parameterization also acts as a source of energy, which increases the TKE of wind flow in wake zone (Figure 5b).

Figure 5: Hub-Height a) Wind Speed and b) TKE Profiles Blue and red lines represent results from the reference (without wind farm) and experiment (with wind farm) simulations, respectively. Gray area is the location of the wind farm.

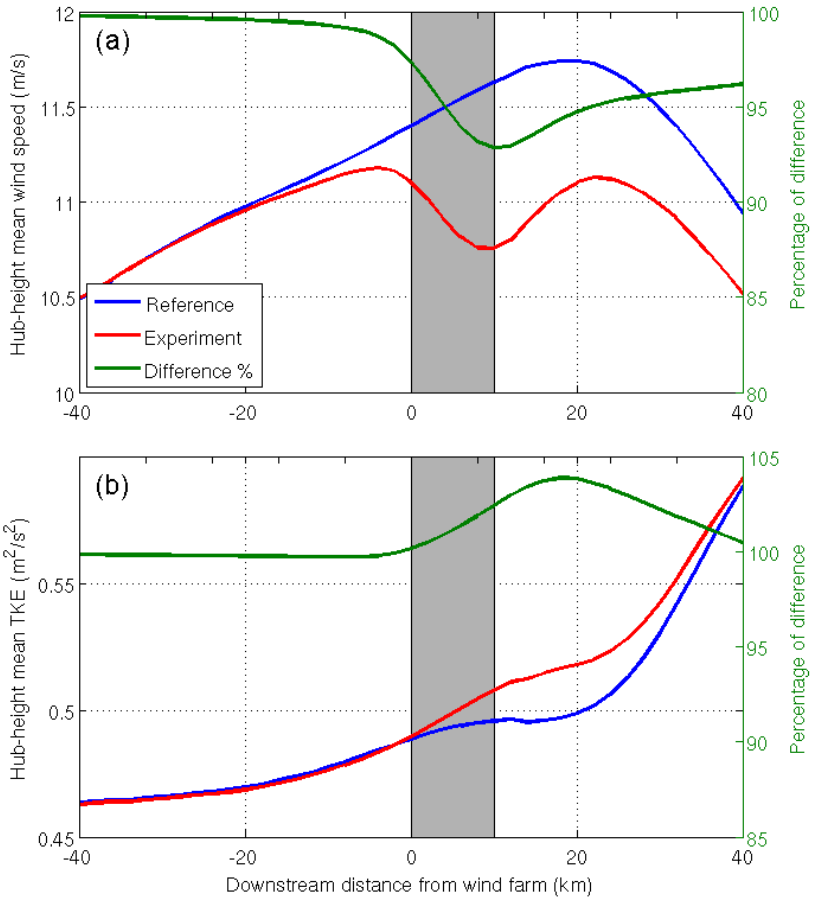

Figure 6 shows wind energy production based on hourly wind speeds and the wind turbine power curve (red line shown at right-bottom corner) released in industrial reports (Vestas 2005, 2013). A diurnal cycle is seen in hourly mean power output shown in Figure 6a (black line, corresponding to the black axes). Wind power production increases from about 900 MWh in the early morning and reaches a peak value of 1030 MWh in the late evening before decreasing around nighttime. A clear seasonal cycle is also seen in daily mean power output per month (blue line, corresponding to the blue axes). Production is higher during the summer months and lower during winter months. Daily main power output in spring and summer (March-August) is about 1.4 times higher than that in fall and winter (September-January). Both curves of hourly output and daily power per month approximately match temporal electricity demand for domestic use.

Figure 6: a) Averaged Hourly Power Output (Black Line, Corresponds to Black Axes) and Averaged Daily Power Output for Each Month (Blue Line, Corresponds to Blue Axes) Provided by the Hypothetical Wind Farm b) Monthly Mean Wind Speed of NARR Data for the Grid Box Containing the Wind Farm

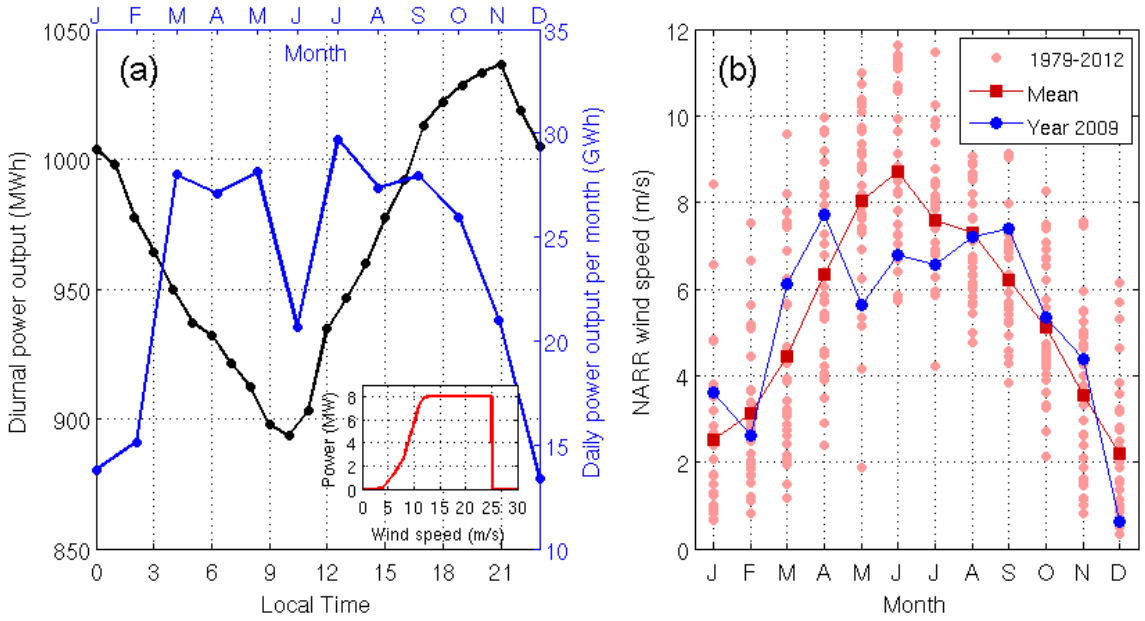

Pink circles and red squares are 1979-2012 data and the climatological mean, respectively. Blue circles are data in the year of the simulation (2009).

Monthly mean hub-height wind speed in NARR data at the location of the wind farm is shown in Figure 6b. The pink circles and red squares are available monthly data and their climatological means from 1979 to 2012, respectively, and the blue markers are data of year 2009. This plot clearly shows that the wind magnitudes in May, June, and July 2009 are much smaller than in corresponding months of most other years and smaller than the climatological mean. Thus, the WRF winds are also unusually small during these particular months, and it is no surprise that less wind power is also generated, as shown in Figure 6a.

According to Figure 6, the designed wind farm is able to provide daily electricity supply for more than 775,000 households, assuming the average daily electricity consumption for a U.S. residential utility customer is about 30 KWh (U.S. Energy Information Administration[4]).

3.2 Meteorological properties above the wind farm

To illustrate the impacts of the hypothetical wind farm, in the following analyses the results are presented in terms of the averaged difference between the experiment (with the wind farm) and reference (without the wind farm) simulations. All results discussed in this section are data from the experimental simulation minus data from the reference simulation. The vertical profiles of changes in key meteorological properties at the wind farm itself are shown in Figure 7. Here the solid line represents the mean difference and the shaded area represents the range of one standard deviation in the difference over the one-year simulation.

Because wind turbines slow wind speed as they extract energy, a significant reduction in wind speed is seen in Figure 7a. As this panel shows, the average reduction is about 0.7 m/s at hub-height, but reduction can be as large as 1.5 m/s for some days. Due to mass continuity, a slight increase in wind velocity is seen above 500 m, the annual mean height of the atmospheric boundary layer top. An increase of shear stress due to the velocity gradient in height triggers a vertical mixing mechanism (Smith, 2009, Baidya Roy et al., 2004) that transfers cooler and more humid air from the ocean surface to the atmospheric boundary layer. As a result, a clear decrease is seen in the vertical profile of air temperature.

The air temperature decrease typically varies from 0.05 to -0.3 K, with a maximum value generally seen at the top of atmospheric boundary layer (Figure 7b). The largest air temperature difference between the experiment and reference simulations can be over 1 K (not visible in figure because only one standard deviation is shown). Meanwhile, the vertical profile of atmospheric humidity shows an opposite trend, due to more water vapor entering the atmospheric boundary layer (Figure 7c). While the vertical mixing mechanism increases the atmospheric boundary layer top by about 10 m (not shown), again due to the enhanced turbulence, more water vapor accumulates inside the atmospheric boundary layer. This leads to enhancement of water vapor condensation to form additional clouds at the top of the boundary layer. The additional condensation may also be due to decreased temperature. Examination of cloud changes, seen in Figure 7d, shows that increased stratocumulus are distributed mainly in the upper part of the boundary layer. The presence of additional clouds will further affect the downward shortwave and longwave radiative fluxes.

[4] http://www.eia.gov/tools/faqs/faq.cfm?id=97&t=3

Figure 7: Vertical Profile of Difference in a) Wind Speed, b) Air Temperature, c) Air Humidity, and d) Cloud Liquid Water Between the Experiment (With the Wind Farm) and Reference (Without the Wind Farm) and Simulations Data are averages from grid points right above the wind farm..

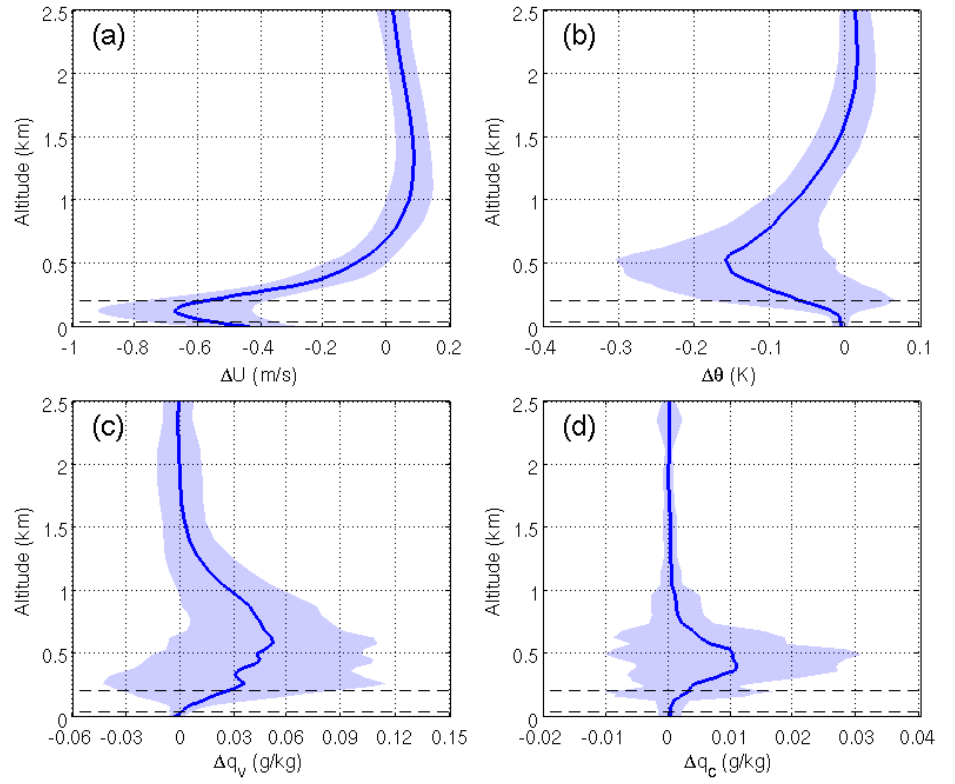

The solid line is the mean value of the differences, while the shaded area represents one standard deviation. The rotor swept area of the wind turbine is bounded by horizontal dashed lines

The changes in velocity, temperature, water vapor, and TKE along the wind farm cross-section is shown in Figure 1. The velocity reduction (Figure 8a) fills the entire marine boundary layer and the wake extends up to about 100 km downstream, as well as temperature reduction (Figure 8b) and water vapor (Figure 8c) excess. Figure 8d shows enhanced TKE due to turbulence shear production remains within the boundary layer. The vertical turbulent mixing causes positive water vapor anomalies and negative temperature anomalies. However, the perturbations above the inversion layer cannot be explained by turbulence transport, which is limited below the inversion layer. Thus, the researchers hypothesize that the temperature and moisture anomalies above the marine boundary layer are results of wind farm-induced standing waves, which is demonstrated by Smith (2009). He found that when the vertical extension of the wind farm-induced velocity deficit is in the order of the boundary layer depth, gravity waves are triggered due to a local shifting of the inversion layer.

Figure 8: Wind Farm Cross-Section of the Differences in a) Velocity, b) Potential Temperature, c) Water Vapor Mixing Ratio, and d) TKE Between the Reference and Experimental Simulations

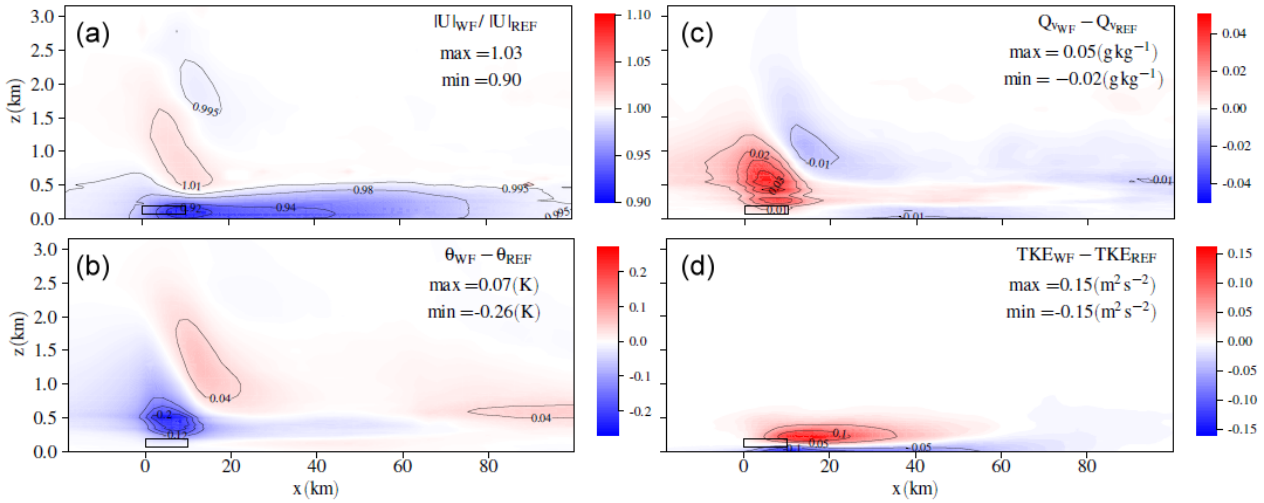

The rectangle indicates the location of wind farm.

3.3 Wind farm-induced wakes and clouds

As shown in Figure 7, significant changes are found in wind speed and boundary layer clouds due to the wind farm. When wind turbines reduce wind speed to extract energy from the airflow through the wind farm, they also generate downstream wakes.

Figure 9a shows a 3D representation of the wake region, representing the percentage of average wind speed reduction. The maximum reduction, about 10 percent, is seen at the southern boundary of the wind farm, and a small range of velocity deficit is also seen upstream of the wind farm. In general, the magnitude of wakes decreases downstream. The zone where wind velocity is reduced by 1.5 percent or more extends more than 100 km downstream from the location of the wind farm to the San Francisco Bay Area. Due to strong inversions in this region, the vertical range of wind farm-induced wakes is limited by the atmospheric boundary layer height, which is about 500 m. The horizontal spread of the wakes extend from about 30 km near the wind farm to about 50 km near the Point Reyes National Seashore, where it starts to be limited by mountain terrain.

Figure 9: 3D Representation of Wind Farm-Induced a) Downstream Wakes (the Percentage of Wind Speed Reduction) and b) Additional Clouds (g/kg)

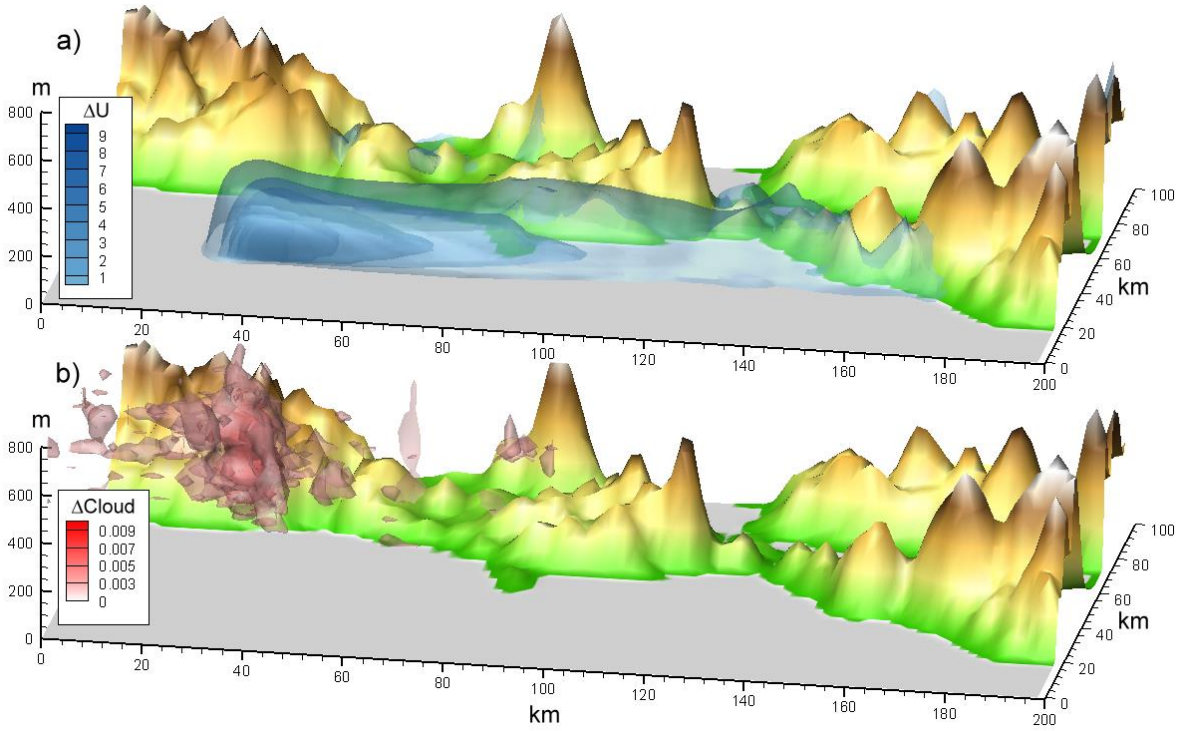

The isosurfaces are the annual average of the difference between the experiment and reference simulation data.

Clouds over the ocean surface in the study domain are typically classified as stratocumulus. The stratocumulus decks can cover thousands of square km and play an important role in regulating local weather and climate (Klein and Hartmann, 1993). Figure 9b shows the 3D distribution of the additional clouds due to the wind farm. While wind-farm induced vertical transport raises the top of boundary layer, it also accumulates extra water vapor to form more stratocumulus at the level of the inversion. Since the strong vertical mixing mechanism is limited to the location of the wind farm, these extra clouds are mainly distributed above the wind farm and surrounding areas, with a peak value right above the atmospheric boundary layer. The annual mean of the peak value in cloud liquid water increase over the wind farm is about 0.09 g/kg. The average increase of cloud due to the wind farm is about 10 percent.

3.4 Near-surface fluxes

The surface energy budget is also strongly affected by decreased wind speeds and increased boundary layer clouds. Figure 10 shows maps of changes in the daytime average incoming radiation and surface turbulent fluxes between the experiment and reference simulations. Because cloud liquid water affects downward radiative fluxes reaching the surface, a clear reduction in incoming shortwave radiation is seen in Figure 10a. This panel shows that the reductions are concentrated at the location of wind farm, with an average value of about 10

W/m^2. Meanwhile, the opposite result is seen in the change of downward longwave radiation (Figure 10b). Compared to the reduction in shortwave radiation, the magnitude of the increase in longwave radiation is smaller; however, with a peak value of about 2.5 W/m^2. Both changes in radiation match the distribution of additional clouds shown in Figure 9b.

Changes in micrometeorological variables, including wind speed reduction, affect surface turbulent fluxes. Figure 10c and 10d show the changes in sensible and latent heat fluxes, respectively, while both turbulent fluxes are functions of near-surface wind speed. Although the reduction in wind speed tends to decrease both surface fluxes, the results show the domination of changes in heat and moisture gradients. As shown in Figure 7b, the wind farm leads to a decrease of air temperature. This results in an increase in the temperature gradient (with identical sea surface temperature), which further increases the magnitude of sensible heat flux (Figure 10c). The maximum average increase in sensible heat flux is about 1 W/m^2, at the southern boundary of the wind farm, while the annual mean of sensible heat flux over the wind farm area in the reference simulation is about 0 W/m^2. On the other hand, the wind farm also leads to additional moisture in the air (Figure 7c), which reduces the humidity gradient and the magnitude of latent heat flux (Figure 10d). The maximum average decrease in latent heat flux is about 5 W/m^2, which is about 15 percent of the annual mean of latent heat flux in wind farm area (about 35 W/m^2). The distribution of changes in sensible and latent heat fluxes clearly follows the wind-farm-induced wake shown in Figure 9a. This result implies that the distribution of wind farm-induced wakes also affects the distribution and propagation of changes in near-surface air temperature and humidity down to the San Francisco Bay. Surface fluxes results shown in this study come from the WRF simulations using prescribed sea surface temperature data. If a coupled simulation including both atmospheric and oceanic models is performed, the changes in surface fluxes may increase.

Figure 10: Map of Differences in a) Incoming Shortwave Radiation, b) Incoming Longwave Radiation, c) Sensible Heat Flux, and d) Latent Heat Flux Between the Experiment (With the Wind Farm) and Reference (Without the Wind Farm) Simulations (Data in the Experiment Simulation Minus Data in the Reference Simulation, W/m^2).

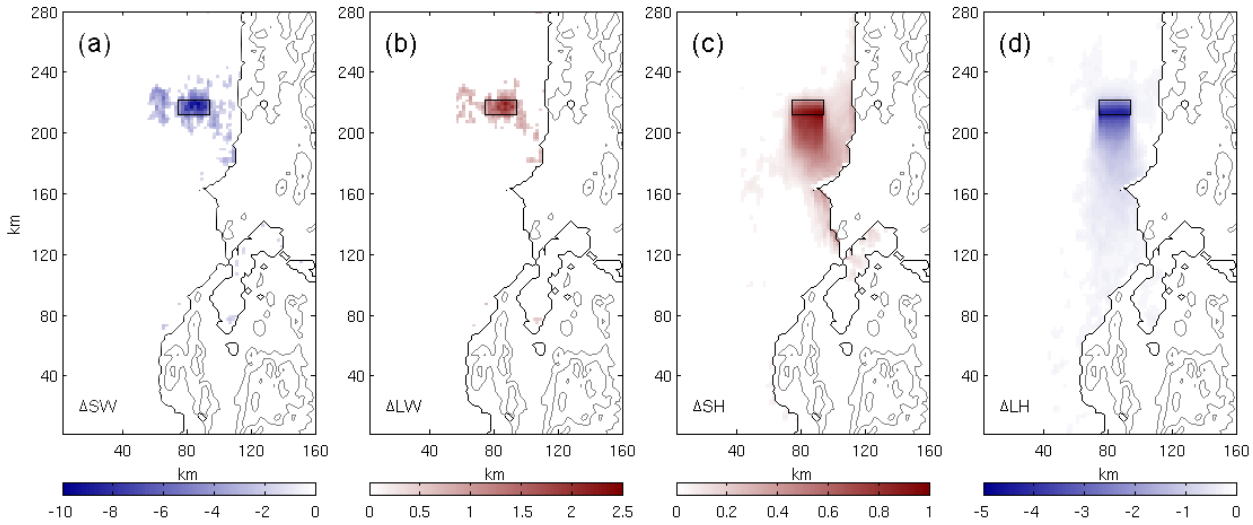

The black box represents the location of the hypothetical wind farm.

CHAPTER 4:
Ongoing Work

Although the local energy demand clearly influences decisions about wind farm designs, including the size of a wind farm and its individual turbines, this study shows that the wind farm-induced impacts on the surrounding environment should also be taken into account. More analyses are needed to quantify the relationship between the wind farm/turbine size and the changes in meteorological variables. As mentioned in the Introduction (Chapter 1), California's coast is a region of ocean upwelling driven by consistent northerly winds. Changes in atmospheric structure downwind from a large offshore wind farm could alter ocean thermal structure, upwelling, nutrient supply, and probably the marine ecosystem. Therefore, in an ongoing work, near-surface atmospheric forcing data will be used to drive a regional ocean model to investigate these effects.

4.1 Regional Ocean Modeling System

The goal is to run a practice simulation of the ocean model – the Regional Ocean Modeling System (ROMS) – to investigate ocean variables such as currents, sea surface temperature, and surface fluxes in the study domain. This allows us to be more familiar with physics structures inside this advanced ocean model and its optimal settings for performing simulations over California's coast.

Figure 11: An Example of ROMS Simulation Result: a Snapshot of Calculated Sea Surface Temperature From Along California's Coast

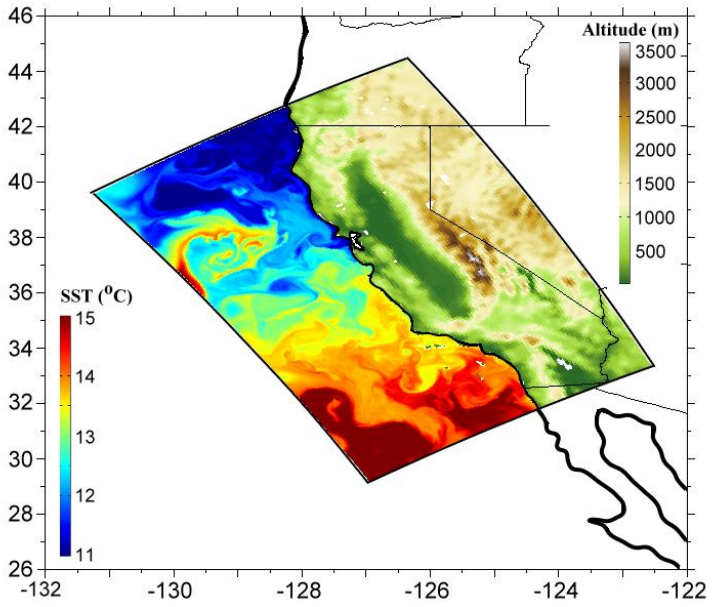

ROMS is a free-surface, terrain-following, primitive equations ocean model used by the oceanic science community for a diverse range of applications. ROMS includes accurate and efficient

physical and numerical algorithms and several coupled models for biogeochemical, bio-optical, sediment, and sea ice applications. It also includes several vertical mixing schemes, multiple levels of nesting, and composed grids. ROMS uses short time steps to advance the surface elevation and barotropic momentum, and a much larger time step is used for calculations of temperature, salinity, and baroclinic momentum. Figure 11 shows an example of ROMS results.

Near the open surface connected to atmosphere (the area of interest in this study), the local closure schemes are based on the Mellor-Yamada level 2.5 TKE equations and the Generic Length Scale parameterization. For a non-local closure scheme, the K-profile planetary boundary layer scheme is used to parameterize the unresolved physical vertical subgrid-scale processes. The sea-air interaction boundary layer in ROMS is based on the bulk parameterization adapted from the Coupled Ocean-Atmosphere Response Experiment algorithm for the computation of surface fluxes of momentum, sensible heat, and latent heat.

Figure 12: ROMS Domain Configuration

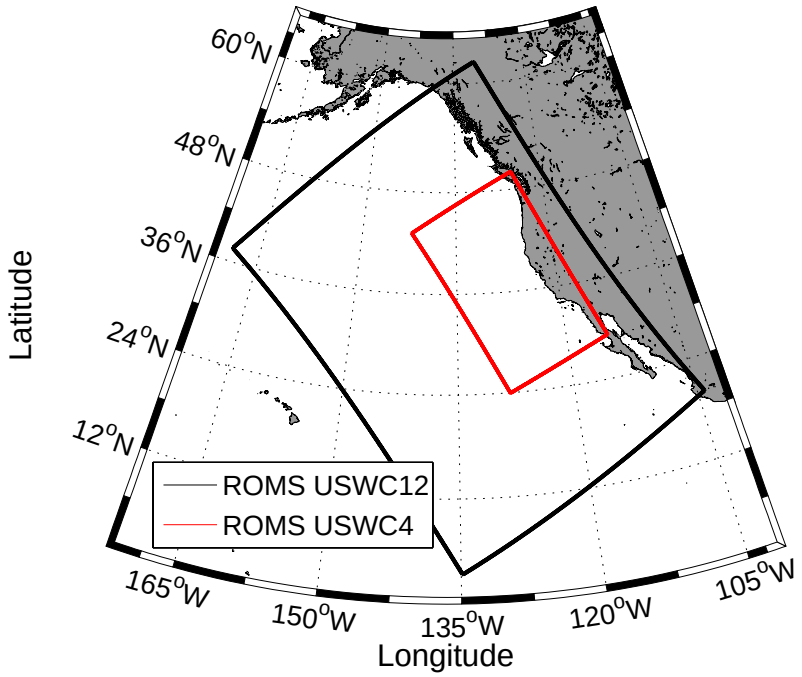

The black (USWC12) and red (USWC4) boxes represent the outer and inner domains with 12 and 4 km grid resolution, respectively.

The oceanic simulations will be performed with ROMS. As shown in Figure 12, the first (outer) domain (black box) covers the entire East coast of the North American continent with a resolution of 12 km, and the second (inner) domain (red box) has a spatial resolution of 4 km, which allows an accurate representation of mesoscale turbulence along the coast. The model has 42 vertical levels and the vertical grid is stretched for increased boundary layer resolution. The finest vertical resolution near the ocean surface varies between 3 to 5 m in different locations. However, this resolution is able to accurately simulate small oceanic eddies in the interface

between sea surface and atmosphere. At the boundaries of the first domain, mixed active-passive conditions are used with the forcing selected from the Simple Ocean Data Assimilation, which provides a data set with a temporal resolution of five days and a spatial resolution of 0.25° by 0.4° with 40 vertical levels. The open-boundary conditions in the inner domains allow for both incoming forcing information from the atmospheric model (i.e., WRF model) to simulate a free evolution of current flows. Subgrid-scale vertical mixing is parameterized using the K-profile planetary boundary layer formulation and the dominant lateral mixing is due to the upstream-biased advection operator. The forcing data from WRF (to ROMS) include reference-level air temperature and specific humidity, surface wind vector (i.e., shear stress), net shortwave and downward longwave radiative fluxes, and precipitation, with a temporal interval of one hour. As a result, ROMS calculates turbulent momentum and heat fluxes using a bulk flux formulation.

In this work, the researchers started to understand the physics structures of ROMS modeling framework and to perform some preliminary simulations to test its ability to calculate sea-surface temperature, surface fluxes, and other related oceanic variables for the study domain of interest. Through such preliminary simulations, the researchers are able to analyze the important variables in the oceanic surface boundary layer. Additionally, the authors can investigate their potential impacts on sea-air interactions and the feedback interacting with proposed wind farm.

CHAPTER 5:
Conclusion

In this work, the researchers propose the placement of a large-scale modern offshore wind farm near the Northern California's coast and investigate its potential impacts on the surrounding atmospheric environment. The WRF framework integrated with a recently developed wind farm parameterization is utilized to perform numerical simulations. Two one-year simulations with and without the wind farm were performed and then compared to advance understanding of the hypothetical wind farm's impacts.

Using one of the largest offshore wind turbines currently on the market, the hypothetical wind farm could provide electricity to meet the daily needs of about three quarters of a million residents in the San Francisco bay area. Recent studies have found that onshore wind farms containing small turbines significantly increase atmospheric mixing and near-surface warming (Baidya Roy et al., 2004; Baidya Roy and Traiteur, 2010; Zhou et al., 2012; 2013; Rajewski et al., 2013; Fitch et al., 2013; Smith et al., 2013). Larger offshore turbines create more mixing within the atmosphere downwind from the wind farm. However, the same mixing mechanism over the sea surface will create different meteorological impacts from those over land. Because cooler, more humid air is mixed upwards in the atmospheric boundary layer, a cooling effect is seen in the simulation. This result matches the global observations of wind farms reported in Wang and Prinn (2011). Furthermore, because of a strong inversion with frequent stratocumulus over the study area, the additional water vapor brought by the wind turbines leads to more condensed water and cloud.

Whereas maximum reductions in wind speed occur at the turbine hub-height, the maximum changes in temperature, specific humidity, and liquid water are seen at the inversion zone. Additional clouds accumulate above the location of the wind farm where incoming radiative fluxes are mainly affected. But the wind farm-induced wakes due to wind speed reduction can extend more than 100 km downstream to the Bay Area. The distributions of changes in air temperature and humidity basically follow the wake propagation and they further affect the distributions of surface turbulent fluxes. This finding matches a recent laboratory experiment study (Zhang et al., 2013).

REFERENCES

Baidya Roy S, Pacala S W and Walko R L 2004 Can large wind farms affect local meteorology? *J. Geophys. Res.* 109 D19101.

Baidya Roy S and Traiteur J J 2010 Impacts of wind farms on surface air temperature *Proc. Natl Acad. Sci.* 107 17899-17904.

Barthelmie R J and Pryor S C 2006 Challenges in Predicting Power Output from Offshore Wind Farms *J. Energy Engr.* 132 91-103.

Calaf M, Meneveau C and Meyers J 2010 Large eddy simulation study of fully developed wind-turbine array boundary layers *Phys. Fluids* 22 015110.

Calaf M, Parlange M B and Meneveau C 2011 Large eddy simulation study of scalar transport in fully developed wind-turbine array boundary layers *Phys. Fluids* 23 126603.

Chamorro L P and Porté-Agel F 2010 Effects of thermal stability and incoming boundary-layer flow characteristics on wind-turbine wakes: a wind-tunnel study *Bound.-Layer Meteorol.* 136 3 515-533.

Chen F and Dudhia J 2001 Coupling an advanced land surface-hydrology model with the Penn State–NCAR MM5 modeling system. Part I: Model implementation and sensitivity *Mon. Wea. Rev.* 129 569-585.

Churchfield M J, Lee S, Michalakes J and Moriarty P J 2012 A numerical study of the effects of atmospheric and wake turbulence on wind turbine dynamics *J. Turbul.* 13 1-32.

Dudhia J 1989 Numerical study of convection observed during the winter Monsoon experiment using a mesoscale two-dimensional model *J. Atmos. Sci.* 46 3077-3107.

Dvorak M J, Archer C L and Jacobson M Z 2010 California offshore wind energy potential *Renewable Energy* 35 1244-1254.

Goesswein J 2010 REpower 6M Hamburg offshore wind conference Hamburg Germany.

Fiedler B H and Bukovsky M S 2011 The effect of a giant wind farm on precipitation in a regional climate model *Environ. Res. Lett.* 6 045101.

Fitch A C, Olson J B, Lundquist J K, Dudhia J, Gupta A K, Michalakes J and Barstad I 2012 Local and mesoscale impacts of wind farms as parameterized in a mesoscale NWP model *Mon. Wea. Rev.* 140 3017-3038.

Fitch A C, Lundquist J K and Olson J B 2013 Mesoscale influences of wind farms throughout a diurnal Cycle *Mon. Wea. Rev.* 141 2173-2198.

Hong S-Y and Lim J J-O 2006 The WRF single-moment 6-class microphysics scheme (WSM6) *J. Korean Meteor. Soc.* 42 129-151.

Huang H-Y, Hall A and Teixeira J 2013 Evaluation of the WRF PBL parameterizations for marine boundary layer clouds: Cumulus and stratocumulus *Mon. Wea. Rev.* 141 2265-2271.

Kain J S 2004 The Kain-Fritsch convective parameterization: An update. *J. Appl. Meteor.* 43 170-181.

Klein S A and Hartmann D L 1993 The seasonal cycle of low stratiform clouds *J. Climate* 6 1587-1606.

Lu H and Porté-Agel F 2011 Large-eddy simulation of a very large wind farm in a stable atmospheric boundary layer *Phys. Fluids* 23 065101.

Jacobson M Z 2009 Review of solutions to global warming, air pollution, and energy security *Energy Environ. Sci.* 2 148-173.

Jacobson M Z and co-authors 2014 A roadmap for repowering California for all purposes with wind, water, and sunlight *Energy* 73 875-889.

Jousse A, Hall A, Sun F and Teixeira J 2014 How do parametrizations affect stratocumuli and surface energy fluxes in WRF? In preparation.

Mesinger F, and co-authors 2006 North American Regional Reanalysis *Bull. Amer. Meteor. Soc.* 87 343-360.

Mlawer E J, Taubman P D, Iacono M J and Clough S A 1997 Radiative transfer for inhomogeneous atmosphere: RRTM, a validated correlated-k model for the longwave *J. Geophys. Res.* 102 16 663-682.

Nakanishi M and Niino H 2004 An improved Mellor-Yamada level-3 model with condensation physics: Its design and verification *Bound.-Layer Meteorol.* 112 1-31.

Porté-Agel F, Wu Y-T, Lu H and Conzemius R J 2011 Large-eddy simulation of atmospheric boundary layer flow through wind turbines and wind farms *J. Wind Eng. Ind. Aerodyn.* 99 4 154-168.

Rajewski D A and co-authors 2013 Crop Wind Energy Experiment (CWEX): observations of surface-layer, boundary-layer, and mesoscale interactions with a wind farm *Bull. Am. Meteorol. Soc.* 94 655-672.

Schwartz M, Heimiller D, Haymes S, and Musial W 2010 Assessment of offshore wind energy resources for the United States Technical Report NREL/TP-500-45889, NREL, Golden, CO.

Seifert G 2007 Idaho Wind Data, Idaho Falls, Idaho National Laboratory.

Skamarock W C, Klemp J B, Dudhia J, Gill D O, Barker D M, Duda M, Huang X-Y, Wang W and Power J G 2008 A description of the Advanced Research WRF Version 3 *NCAR Technical Note* NCAR/Tech Notes-475+STR 125 pp.

Smith R B 2009 Gravity wave effects on wind farm efficiency, *Wind Energy*, 13 449-458.

Smith C M, Barthelmie R J and Pryor SC 2013 In situ observations of the influence of a large onshore wind farm on near-surface temperature, turbulence intensity and wind speed profiles, *Environ. Res. Lett.* 8 034006.

US Department of Energy 20% Wind by 2030 2008 DOE/GO-102008-2567 available at http://www1.eere.energy.gov/wind/pdfs/42864.pdf.

Vestas Wind Systems A/S 2005 General Specification V80-1.80 MW.

Vestas Wind Systems A/S 2013 Lowering the cost of energy offshore V164-8.0 MW.

Volker P J H, Badger J, Hahmann A N and Ott S 2014 Implementation and evaluation of a wind farm parameterization in a mesoscale model *Bound.-Layer Meteorol.* in revision.

Wagner R, Antoniou I, Pedersen S M, Courtney M S, and Jorgensen H E 2009 The influence of the wind speed profile on wind turbine performance measurements *Wind Energy* 12 348-362.

Wang C and Prinn R G 2011 Potential climatic impacts and reliability of large-scale offshore wind farms, *Environ. Res. Lett.* 6 025101.

Weinzettel J, Reenaas M, Solli C and Hertwich E G 2009 Life cycle assessment of a floating offshore wind turbine *Renewable Energy* 34 3 742-747.

Wharton S and Lundquist J K 2010 Atmospheric stability impacts on power curves of tall wind turbines - An analysis of a west coast North American wind farm LLNL-TR-424425.

Wu Y.-T. and Porté-Agel F 2011 Large-eddy simulation of wind-turbine wakes: evaluation of turbine parameterizations *Bound.-Layer Meteorol.* 138 3 345-366.

Wyngaard J C 2010 *Atmospheric Turbulence* Cambridge University Press New York 393 pp.

Zhang W, Markfort C D and Porté-Agel F 2013 Experimental study of the impact of large-scale wind farms on land–atmosphere exchanges, *Environ. Res. Lett.* 8 015002.

Zhou L, Tian Y, Baidya Roy S, Thorncroft C, Bosart L F and Hu Y 2012 Impacts of wind farms on land surface temperature *Nature Climate Change* 2 539-543.

Zhou L, Tian Y, Baidya Roy S, Dai Y and Chen H 2013 Diurnal and seasonal variations of wind farm impacts on land surface temperature over western Texas, *Clim. Dyn.* 41 307-326.